

ViSE: Vision-Based 3D Real-Time Shape Estimation of Continuously Deformable Robots

Hehui Zheng^{*1,2}, Sebastian Pinzello^{*1}, Barnabas Gavin Cangan¹, Thomas Buchner¹, Robert K. Katzschmann¹

Abstract—The precise control of soft and continuum robots requires knowledge of their shape. The shape of these robots has, in contrast to classical rigid robots, infinite degrees of freedom. To partially reconstruct the shape, proprioceptive techniques use built-in sensors resulting in inaccurate results and increased fabrication complexity. Exteroceptive methods so far rely on placing reflective markers on all tracked components and triangulating their position using multiple motion-tracking cameras. Tracking systems are expensive and infeasible for deformable robots interacting with the environment due to marker occlusion and damage. Here, we present a regression approach for 3D shape estimation using a convolutional neural network. The proposed approach takes advantage of data-driven supervised learning and is capable of real-time marker-less shape estimation during inference. Two images of a robotic system are taken simultaneously at 25 Hz from two different perspectives, and are fed to the network, which returns for each pair the parameterized shape. The proposed approach outperforms marker-less state-of-the-art methods by a maximum of 4.4% in estimation accuracy while at the same time being more robust and requiring no prior knowledge of the shape. The approach can be easily implemented due to only requiring two color cameras without depth and not needing an explicit calibration of the extrinsic parameters. Evaluations on two types of soft robotic arms and a soft robotic fish demonstrate our method’s accuracy and versatility on highly deformable systems in real-time. The robust performance of the approach against different scene modifications (camera alignment and brightness) suggests its generalizability to a wider range of experimental setups, which will benefit downstream tasks such as robotic grasping and manipulation.[†]

I. INTRODUCTION

Soft robots are experiencing a steep rise in popularity thanks to their ability to solve challenges such as compliant grasping and dexterous movement [1]–[3], tasks with which rigid robots typically struggle [4]. To fully exploit the capabilities of soft robots, modern control approaches are needed, which typically rely on rich state feedback. However, obtaining and accurately describing the state of a continuously deforming soft body or robot is challenging compared to the state of a rigid object or robot. Encoders at the connecting joints of rigid robots readily provide precise state measurements, while soft robots mostly consist of elastomeric materials that deform with infinite degrees of freedom [5]. It is, therefore, crucial to solve the challenge of soft robotic state estimation to exploit the full potential of the great variety of soft robots for manipulation and beyond.

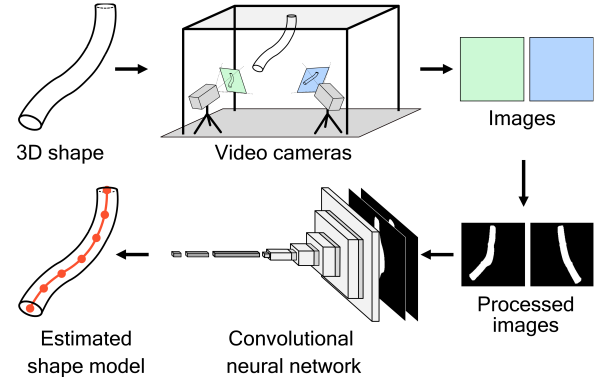


Fig. 1. Diagram of the real-time marker-less inference pipeline for the proposed shape estimation approach ViSE. A 3D shape is captured by two RGB video cameras. Image pairs are preprocessed and run through a convolutional neural network to estimate a shape model for the 3D shape.

To date, various shape estimation approaches have attempted to improve soft robotic sensing capabilities. One type of sensing approach uses mechanical proprioception similar to classical robotic state estimation [6]–[9]. A variety of sensor types such as resistive, capacitive, optical, and pneumatic transducers proprioceptively estimate the continuous deformations of soft robots [10]–[12]. Mechanical proprioception with built-in sensors is limited by spatial resolution and increased fabrication complexity. This limitation has lately led to an increased popularity of exteroceptive sensing approaches that are purely vision-based [13]–[15].

A widely applied vision-based method for shape estimation and tracking employs motion-capture systems [13], [16]–[18]. These systems rely on placing reflective markers on an object and triangulating the marker position using multiple calibrated motion-tracking cameras. Such marker-based approaches offer high temporal and spatial resolutions of the placed markers. However, these tracking systems are usually costly and limited in use, hindering the application of marker-based robots in commercial settings where multiple robots are deployed simultaneously within clutter [19]. Motion-capture systems require the tedious placement of many markers on any object to be tracked, which is not a feasible option when working with high-dimensional robotic systems that interact with an environment. Markers cannot be placed too close to each other, limiting the fidelity of shape reconstruction. Furthermore, obstacles could occlude and eventually displace or destroy the markers. Therefore, much research has gone into replacing marker-based approaches by developing marker-less sensing techniques [12], [14], [20]–[24]. Current marker-less approaches still require scenario-

^{*}Equal contribution. Work done at Soft Robotics Lab, ETH Zürich. Correspondence hehui.zheng@ai.ethz.ch

¹Soft Robotics Lab, ETH Zürich, Zürich, Switzerland;

²ETH AI Center, Zürich, Switzerland.

[†]All code available on <https://github.com/srl-ethz/vise>.

specific capturing setups and strict formatting requirements of the image data.

In this work, we choose an approach towards 3D shape estimation of continuously deformable robots that leverages data-driven deep learning. We propose ViSE, a Vision-based regression approach for camera-based, 3D Shape Estimation using a convolutional neural network (CNN) (Figure 1). The performance of our real-time shape estimation is compared against marker-based motion capture in the tasks of estimating the shape of soft robotic arms and soft robotic fish.

Specifically, our work provides the following contributions:

- We present a simple-to-implement approach using two cameras and applicable to various soft robots.
- We employ an adaptive image processing pipeline that does not require specific lighting conditions or flawless background removal.
- We demonstrate the real-time estimation capability of our system, which enables its use for downstream applications such as the closed-loop control of soft robots.

Section II summarizes related work and Section III presents our methodology. In Section IV, we provide evaluation results to exhibit the performance of the proposed CNN-based approach and discuss the estimation accuracy under different model assumptions. Finally, Section V concludes the work and outlines directions for future research.

II. RELATED WORKS

Previous works demonstrate vision-based continuous shape estimation approaches that either necessitate strict image requirements or work only for specific setups. In the following, we briefly discuss the most related works, focusing on marker-less shape estimation approaches.

Hannan and Walker use basic image processing techniques, including thresholding and image segmentation, to estimate the 2D shape of a planar, cable-actuated elephant trunk manipulator from single images [20]. However, their estimation results are only compared to another cable-based shape estimation technique but not with actual ground truth. Camarillo et al. extend the computer-vision methods to 3D shape estimation of a thin continuum manipulator [21]. If the precise positions of cameras are known, they could extract silhouettes from multiple cameras' views, project those silhouettes into a volumetric space to find their intersection, and fit a spline through the resulting 3D point cloud. This approach requires a strong contrast between the tracked shape and the background, as well as the absence of other objects in the field of view.

Strict requirements on the image data are also found in other works. AlBeladi et al. rely on successful edge detection of their soft arm to fit a geometric strain-based model to these edges [14]. Croom et al. also perform edge detection, but then fit reference points to the edges by using an unsupervised learning algorithm called the self-organizing map [22]. All of these approaches show good estimation results but require a strong contrast between the tracked object and the background.

Vandini et al. extract and join straight lines from a monoplane fluoroscopic surgical image to estimate the shape

of a concentric tube robot [24]. By posing conditions for connecting the line features, they manage to relax image requirements and can extract curves from more unclear image data compared to the aforementioned works [25]. Reiter et al. [26] take on a similar approach to ours in that they extract features from segmented binary stereo-images. Since their feature extraction pipeline relies on the color-coded segments of their continuum robot, it does not generalize to other types of robots that do not have those features.

Mathis et al. created a deep learning framework based on transfer learning for marker-less pose estimation and tracking called DeepLabCut [27]. Their framework enables tracking of multiple visual features in unprocessed videos using only a small number of labeled frames for training. They demonstrate their method by tracking body parts of mice and show that they achieve pixel tracking errors comparable to human-level labeling accuracy. However, this framework by itself is restricted to pixel tracking in an image, and it cannot directly track 3D coordinates of features.

Our approach for 3D shape estimation of continuously deformable robots employs convolutional neural networks. While there are many vision-based proprioceptive methods for soft robots using deep learning [28]–[30], we focus on exteroceptive approaches that are simple to implement and do not add complexity to the manufacturing of the soft robots.

III. METHODS

Our proposed shape estimation method is a learned multi-view shape estimation from grayscale images. First, different views of the desired object are captured by two cameras. Then, unnecessary information in the images is removed by an image processing pipeline that transforms them into binary images. The processed images are then fed into a convolutional neural network (CNN) trained to estimate the parameters of the shape representation. The approach is outlined in Figure 1 and the following subsections detail the sub-components of our method.

A. Image Preprocessing

The RGB images of the shape are preprocessed to facilitate the learning procedure. The original images are converted to grayscale, cropped around the shape, and scaled to the size of 256×256 pixels. This preprocessing preserves enough information to accurately represent the shape, while keeping the number of parameters of the CNN relatively small. A median filter with a 7×7 pixel kernel size is applied to reduce noise before using adaptive thresholding to reduce the grayscale image to a binary image [31]. This step removes the background variations while preserving the shape. In addition, the adaptive nature of the thresholding operation and the resulting binary images make our trained network function in a wide range of lighting conditions without the need for retraining. Erosion and dilation with a 7×7 pixel kernel are applied for three iterations each to remove the remaining artifacts.

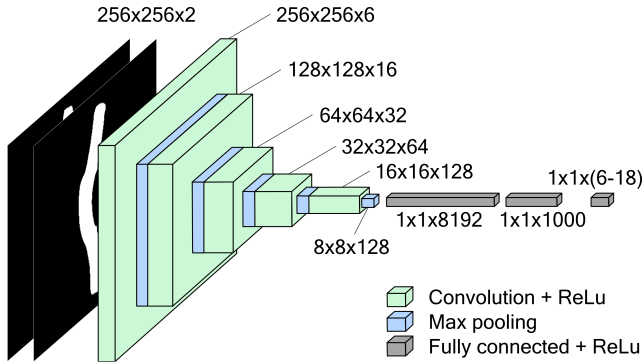


Fig. 2. CNN Network Architecture used in ViSE. Inputs are the pre-processed images from both cameras, and output sizes depend on the selected shape representation and robot.

B. Network Architecture

The CNN used in this work is adapted from the VGG architecture [32]. Since our approach uses binary images, we can take advantage of the simplicity and versatility of VGG. To reduce the computational demand further and improve real-time performance, several convolutional layers are removed from the standard VGG network. The final softmax layer is also removed to perform a regression instead of a classification. The architecture of our network is illustrated in Figure 2.

The network’s main elements are convolutional layers, batch normalization, rectification (ReLU) nonlinearities, and max pooling operations. These elements are applied in the mentioned order and repeated five times before the output is fed into two fully connected layers. All five convolutional layers have a kernel of size three, a stride of one, and a padding of one. The number of channel dimensions is increased from 2 to 6, 16, 32, 64, and 128. Batch normalization is applied before each convolutional layer. Every max-pooling operation reduces its input by a factor of two, reducing the initial image size of 256×256 pixels to 8×8 pixels after five operations. Hence, the input to the first fully connected layer is of size $8'192$ ($8 \times 8 \times 128$). A ReLU nonlinearity is applied after the first fully connected layer. The input to the last fully connected layer has a size of $1'000$, which is reduced to the output of size of either 6, 9, 12, or 18, depending on which shape representation and data set are used.

C. Shape Representations

We consider two different shape representations, the point, and piecewise constant curvature (PCC) model. The point representation comprises the positions of the key points along the soft robots. Using the motion capture software (*Qualisys Track Manager*), virtual coordinate frames are placed at the center of each group of motion markers to line up with the corresponding segment’s centroid. These coordinate frames allow the tracking of not only each segment’s translation but also orientation. We then choose to fit the PCC model [33], [34], a commonly used kinematic reduction model in soft robotics, to these virtual coordinate frames. This PCC model allows the modeling of a continuous shape by approximating

it with multiple constant-curvature sections of fixed length. Each section is defined by two parameters, the curvature and an angle indicating the curving direction. Hence, the model only requires a few parameters to represent a long, continuously deformable shape, which is useful for model-based control purposes.

D. Camera Realignment

No explicit camera calibration is needed and the camera configuration is implicitly learned by the CNN. This design choice limits the cameras’ positions to be fixed relative to the soft robot during the data collection. To alleviate the need for retraining, fiducial markers (*AprilTags*) [35] are attached to the robot’s base. The camera’s translation and rotation relative to the base can be extracted from the image of the fiducial markers. Our realignment utility for the camera pose compares the camera’s current and previously saved positions relative to the fiducial markers. With this utility, users can set up the RGB cameras close to the configuration they were set up during data collection and reuse the trained CNN repeatedly.

While this supervised approach still requires a motion capture setup to initially collect the ground truth data for training, the cameras can be moved without requiring re-training. A user can realign their cameras to approximately match the original poses relative to the robot’s base and still perform inference using the original training data. Given our realignment utility, the trained model still successfully estimates the shape of the robot without requiring a motion capture system.

IV. REAL-WORLD EXPERIMENTS

A. Experimental Setup

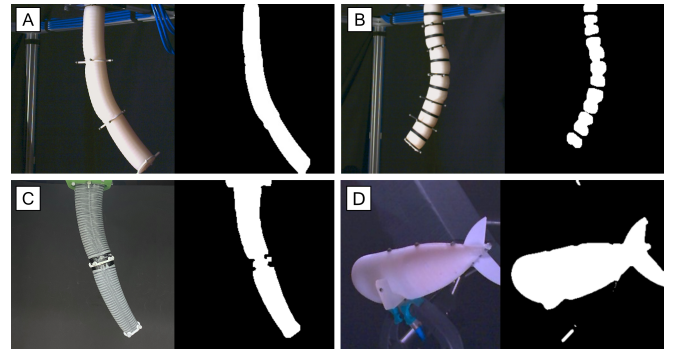


Fig. 3. Soft robots used for performance evaluation, in each panel, left shows the original RGB image, right shows the preprocessed image. A. *WaxCast* Arm [18]. B. *WaxCast* arm with visual features (black stripes) [18]. C. *SoPrA* arm [36]. D. Soft fish [37].

1) *Soft Robots for Evaluation*: The approach is tested on two types of soft robotic arms [18], [36], [38] and a soft robotic fish [37], [39] (Fig. 3). The first soft robotic arm (which we shall refer to as the *WaxCast* arm) consists of three axially connected cylindrical segments, each with four separately inflatable chambers. They are inflated using air provided through a pressure-controlled valve array (*Festo SE & Co. KG*). By inflating one side, the chambers on that

side elongate and induce bending in the segment, thus, the bending direction of the arm can be chosen by selecting the corresponding combination of inflation chambers. Each segment has a length of about 110 ± 1 mm and a diameter of 40 ± 1 mm. The combined length of the arm is 335 ± 3 mm. The second arm, *SoPrA*, is a two-segment soft robotic arm with fiber-reinforced pneumatic actuators. Segments are made of three individually fiber-reinforced elastomer air chambers that are glued together. Combining two of these segments adds up to a total length of 268 ± 2 mm. The robotic fish tail is similar in construction and actuation compared to the *WaxCast* arm, except that it is shaped like a fishtail. It consists of two inflatable chambers and has a total length of 115 ± 1 mm.

2) *Data Collection*: The ground truth data for learning is obtained by eight *Miquis M3* motion-capture cameras from *Qualisys AB* placed in the motion capture space of $1.6 \times 1.1 \times 0.8$ m. The placement of the motion-capture markers can be seen in Figure 3. A group of reflective markers is placed on a rigid ring at the end of every segment of the soft arms. Along the soft fish’s tail, the markers are placed with spaces of 38 ± 1 mm between them. Marker position data is supplied at 100 Hz with an average accuracy of 0.1 ± 0.2 mm, while RGB image data is recorded at 25 Hz by two depth cameras (*Intel RealSense D435i*) [40]. During the data acquisition, the robot’s workspaces are traversed as fully as possible. The segments of the *WaxCast* arm are all actuated to perform a circular motion, with periods of 100, 10, and 1 second, for segments 1, 2, and 3, respectively. We created two data sets, one with three motion-capture marker rings on the arm and the other with six, which also contain visual features in the form of black stripes that were put on the arm (Figure 3B). This process was repeated for *SoPrA*, but the chambers of the arm were randomly actuated. In total, three labeled data sets are generated for two arms, each containing 12’000 poses. The soft robotic fish is actuated to perform a tail-fin stroke with maximal deflection, resulting in a data set of 1’800 poses. Each data set is split into 90% training and 10% testing sets.

3) *Network training*: The network is implemented and trained using the *PyTorch* framework. *AdamW* is chosen as an optimizer and used to minimize the mean absolute loss. The network is trained using a batch size of 64 with an early stop for a maximum of 450 epochs on each data set. The learning rate is set to 10^{-4} and reduced by 0.5 after each 200th epoch. Dropout is applied with a probability of 0.5 in the fully connected layers during training to avoid overfitting. Training on a GPU (Nvidia GeForce RTX 3090) requires between 30 to 60 minutes to converge.

B. Results

1) *Shape Representations*: The CNN was trained using the image data and either learned to output parameters of a PCC model that was fitted to the ground truth marker data or virtual marker positions along the arm (point estimation). We also analyze the approach’s accuracy when estimating just three PCC sections or virtual points compared to estimating six PCC sections or points. Both PCC and point estimation approaches were tested using the data sets from

TABLE I
ESTIMATION ERRORS OF THE PIECEWISE CONSTANT CURVATURE (PCC)
AND POINT ESTIMATION APPROACHES.

Exp.	Repr.	Sec. [§]	Feat.	Point 1 [‡]	Point 2	Point 3 (tip)
A	PCC	6	Yes	$0.9\% \pm 0.3\%$	$3.2\% \pm 1.4\%$	$6.1\% \pm 2.4\%$
B	PCC	3	No	$1.3\% \pm 0.6\%$	$2.6\% \pm 1.3\%$	$6.8\% \pm 3.5\%$
C	Point	6	Yes	$0.06\% \pm 0.03\%$	$0.12\% \pm 0.07\%$	$0.4\% \pm 0.3\%$
D	Point	3	No	$0.4\% \pm 0.4\%$	$0.8\% \pm 1.1\%$	$3.6\% \pm 5.0\%$
E	Point	3	Yes	$0.06\% \pm 0.03\%$	$0.12\% \pm 0.06\%$	$0.3\% \pm 0.2\%$

[§] For 6 sections, only every other section evaluated ^{||} visual features

[‡] Distance error normalized with the robot’s length ($335\text{mm} \pm 3\text{mm}$)

our two *WaxCast* arms (Figure 4A-D). Detailed results of the evaluation can be seen in Table I Exp. A-D, with the point estimation approach strictly outperforming the PCC approach. The errors are normalized based on the robot’s length, which is $335 \text{ mm} \pm 3 \text{ mm}$ for the soft arm.

2) *Visual Features*: To evaluate the effect of visual features on the estimation accuracy, the point estimation approach is applied to a dataset with features (Figure 4E). To create these features, we modified the *WaxCast* arm’s appearance to have multiple black stripes perpendicular to the arm’s backbone (Figure 3B). In Table I, Exp. D and E show that the mean tip error for the feature-less *WaxCast* arm is $3.6 \pm 5.0\%$ and only $0.3 \pm 0.2\%$ for the arm with features.

3) *Benchmarks*: We compared the results of our point estimation approach with four similar works on soft robotic state estimation (see Table II) [14], [21], [24], [41]. Those works also estimated reference points along continuously deforming shapes. Due to limited data from the benchmarks, we only compared the tip errors, which are usually the largest. We believe that achieving low tip position reconstruction error is important for soft robotic shape estimation methods since this accuracy is critical in real-world operations involving reaching and grasping of objects. For a fair comparison, the errors are normalized with the length of each corresponding robot.

DeepLabCut [27] is not included in Table II because it estimates pixel locations instead of 3D positions. To compare our results with *DeepLabCut*, we projected the estimated and ground truth 3D positions into the input images and evaluated the pixel distance error. Exp. C in Table I showed a root-mean-square error at the tip position of 1.13 pixels in one camera view and 1.18 pixels in the other. In comparison, *DeepLabCut* achieved an accuracy similar to the human labeling error of 2.69 ± 0.1 pixels. However, comparing pixel errors is only of limited value, since a pixel error can have a different significance depending on the image resolution and scale of the captured object. Moreover, reprojecting the estimated pixels from multiple calibrated cameras back into 3D space may bring in additional errors due to camera calibrations. Therefore we believe that a direct 3D position estimation is more useful and convenient for downstream applications.

4) *Maximum Estimation Errors*: The maximum estimation errors are computed as an indication of the “worst case scenarios”. For *WaxCast* arm with features, the maximum tip

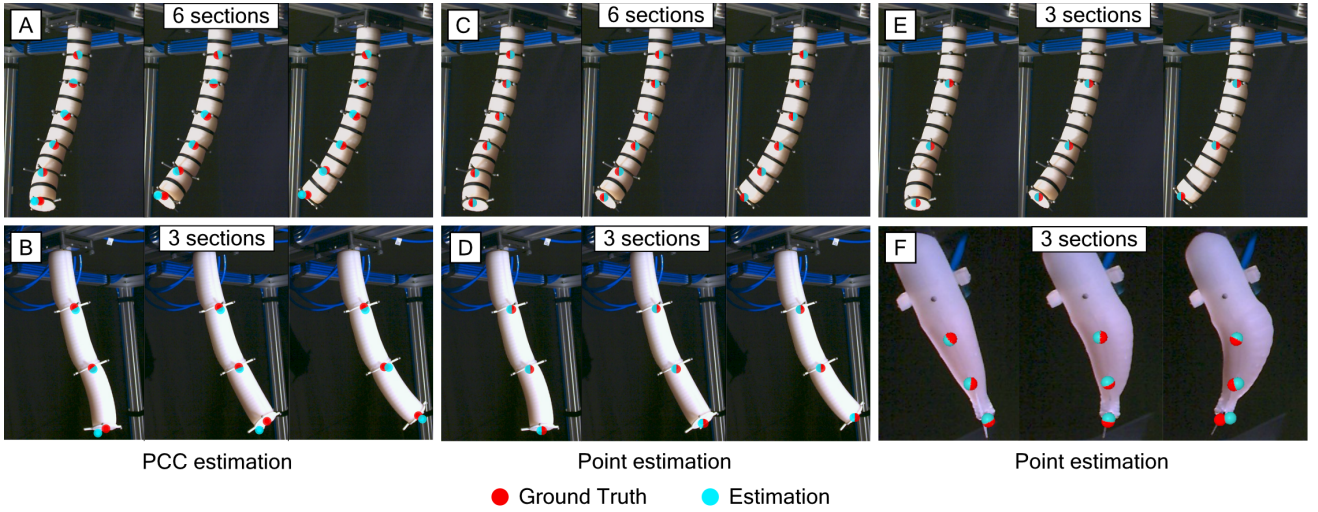


Fig. 4. Estimation results of ViSE compared to ground truth positions. Exp. A, and B employ piecewise-constant curvature (PCC) model, while Exp. C-E estimate the positions of characteristic points separately. The number of sections considered in each experiment is shown in the figure. The red dots mark the ground truth positions obtained by the motion capture system and the blue dots mark the position estimated by ViSE.

TABLE II
ESTIMATION ERRORS OF OUR APPROACH COMPARED TO OTHER WORKS.

	Estimation Technique	Number of Cameras	Flawless Segmentation	Good Contrast	Shape Agnostic	Robot Type	Robot Length (mm)	Tip Error [†]
ViSE (ours)	CNN	2	No	Required	Yes	WaxCast arm	335	0.4% \pm 0.3%
ViSE (ours)	CNN	2	No	Required	Yes	SoPrA	270	1.1% \pm 0.6%
ViSE (ours)	CNN	2	No	Required	Yes	Soft fish	115	2.8% \pm 2.3%
Camarillo et al. [21]	2D point-cloud fit	3	Required	Required	No	Soft arm	160	4.8%
Vandini et al. [24]	Line feature detector	1	No	Required	No	Soft arm	260	2.8%
Pedari et al. [41]	LED light placement	2	No	Required	Yes	Soft arm	468 [¶]	4.5%
AlBeladi et al. [14]	Edge detection & curve fit	1	Required	Required	No	Soft arm	287	4.5% \pm 3.1%

[†] Distance error normalized with the corresponding robot's length

[¶] not provided, calculated based on their estimation data

error is 2.6%, for *SoPrA*, it is 4.3%, and for the soft robotic fish, it is 9.5%.

5) *Online Estimation*: The real-time estimation performance of ViSE was tested on a portable computer (Intel Core i7-7500U @ 2.70 GHz). A mean estimation rate of 18.4 Hz was achieved on this system. Compared to human visual perception time of around 150 ms to 200 ms [42], a single estimation update of our approach takes 54 ms on average, of which 60% are used for the CNN forward calculation and 38% are used for image processing. The remaining 2% are used to stream the images from the RGB cameras.

6) *Different Experimental Setups*: To demonstrate the robust performance of our trained CNN in a range of lighting conditions without the need of retraining, we evaluate and present the tip estimation errors on the *SoPrA* testing data set with modified brightness levels (see Figure 5). The brightness of the original images is modified by adding or subtracting pixel values from the grayscale images (pixel value range 0-255). The experiments are conducted on the *SoPrA* data set since the gray color of the *SoPrA* arm is the closest to the black background. *SoPrA* provides the least contrast

compared to the other soft robots and is, therefore, more sensitive to changes in brightness.

The performance of the trained network is also tested after the reassembly of the cameras. With relative camera translations and orientations obtained from the fiducial markers, we manually realign the cameras to a configuration with 1.46 mm difference from the one used during data collection. The new tip estimation error after reassembly of the cameras is $2.2 \pm 2.4\%$ for the *SoPrA* test data set.

C. Discussion

The results show that the estimation errors increase along the shape regardless of the data set or shape representation being used. The reason for this increase is most likely due to the fact that the tips of these shapes typically move faster and across a larger space than the rest of their shapes. A dynamic behavior increases the estimation difficulty towards the tip.

The approach using the PCC shape representation as output produces larger estimation errors on the three tested data sets (Table I). This error is partially because the endpoint

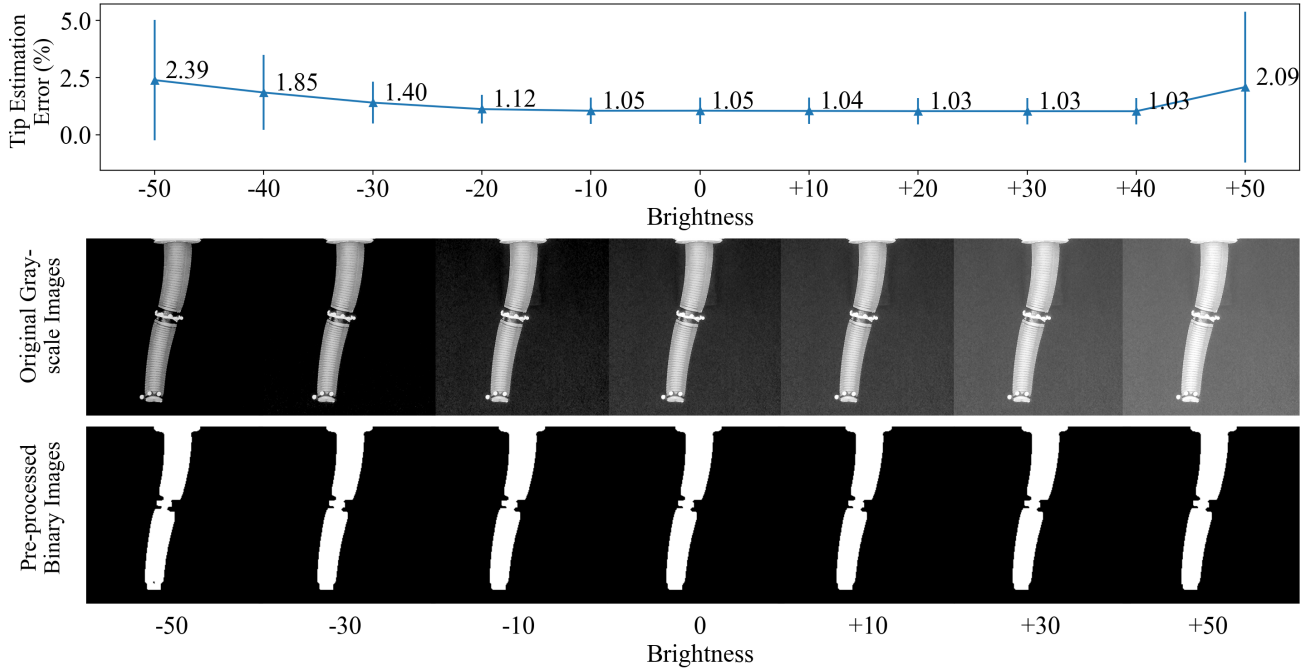


Fig. 5. Tip estimation errors with varying image brightness. The brightness modification is quantified by the addition or subtraction of pixel values (0 – 255) from original grayscale images. Sample grayscale and binary images are shown at different brightness levels.

positions are computed using forward kinematics calculation with all previous PCC sections, which accumulates the estimation errors of each section. Another reason for the inferior performance of the PCC approach is that the constant curvature assumption is sometimes inaccurate for a real soft robotic system. For example, the sections of the soft arm do not exactly bend with constant curvature. The arm’s weight and dynamics, the design characteristics of the inflation chambers, and the fabrication errors all introduce imperfections with regard to the constant curvature assumption. Moreover, the arms we use in this work do not contain an inextensible backbone and therefore also extend along their center line under inflation. This limitation could be resolved by augmenting the PCC model to allow for constant curvature sections of variable length. The CNN would then need to be adjusted to also estimate the length of each segment. However, the error due to non-constant curvature deformation would remain. By estimating points separately, we could avoid both the error accumulation and the PCC model limitations. Although the point representation does not contain any statements about connectedness or directionality, it gives a more precise estimation of the tip position.

The visual features added to the *WaxCast* arm greatly improved the estimation accuracy. This can be seen when comparing Experiments D and E in Table I. We believe that the added features helped the CNN extract more information from the input images. The increased information content improved the deduction of the shape parameters.

We outperform the benchmarks for both soft arms and achieve slight performance improvements for the soft fish, as shown in Table II. At the same time, our approach also does not require flawless shape segmentation or prior

shape knowledge, suggesting the possible generalizability to different types of soft robots.

One limitation of using convolutional neural networks is that the trained network may not be reusable and needs retraining when the experimental setup changes. We tested our trained network on input images with various levels of brightness and also after reassembly of the cameras. The stable performance under brightness changes (Figure 5) indicates that the network could work with a wide range of lighting conditions without re-training as long as there is sufficient contrast for the adaptive image preprocessing. Although retraining would be needed for different camera configurations, we show with the aid of fiducial markers (*AprilTags*), rough realignment to previous camera positions is possible and the trained network can be reused.

V. CONCLUSIONS AND FUTURE WORK

ViSE is a vision-based, 3D soft robot shape estimation approach using two cameras and a CNN. It outperforms current marker-less shape estimation approaches when evaluated on two soft robotic arms and one soft robotic fish. While we consider the visual robustness of our approach to be an improvement over the state-of-the-art, it could be further enhanced to be calibration-free, deal with occlusions, and allow for more expressive representations. Future work will introduce artificial occlusions in the network’s training process to work with partially occluded images and also employ learning-based shape segmentation to perform robust background removal under insufficient contrast. Another future direction is to generalize the approach to the estimation of more expressive kinds of shape representations, *e.g.*, mesh reconstructions, instead of being limited to the estimation of piecewise constant curvatures or characteristic points.

REFERENCES

- [1] Y. Yamanaka, S. Katagiri, H. Nabae, K. Suzumori, and G. Endo, "Development of a food handling soft robot hand considering a high-speed pick-and-place task," in *2020 IEEE/SICE International Symposium on System Integration (SII)*. IEEE, 2020, pp. 87–92.
- [2] Z. Wang, K. Or, and S. Hirai, "A dual-mode soft gripper for food packaging," *Robotics and Autonomous Systems*, vol. 125, p. 103427, 2020.
- [3] S. Abondance, C. B. Teeple, and R. J. Wood, "A dexterous soft robotic hand for delicate in-hand manipulation," *IEEE Robotics and Automation Letters*, vol. 5, no. 4, pp. 5502–5509, 2020.
- [4] E. W. Hawkes, C. Majidi, and M. T. Tolley, "Hard questions for soft robotics," *Science robotics*, vol. 6, no. 53, p. eabg6049, 2021.
- [5] O. Yasa, Y. Toshimitsu, M. Y. Michelis, L. Jones, M. Filippi, T. Buchner, and R. K. Katzschmann, "An Overview of Soft Robotics," *Annual Review - Control Robotics Autonomous Systems*, 2022.
- [6] M. Totaro, A. Mondini, A. Bellacicca, P. Milani, and L. Beccai, "Integrated simultaneous detection of tactile and bending cues for soft robotics," *Soft robotics*, vol. 4, no. 4, pp. 400–410, 2017.
- [7] A. B. Dawood, H. Godaba, and K. Althoefer, "Modelling of a soft sensor for exteroception and proprioception in a pneumatically actuated soft robot," in *Annual Conference Towards Autonomous Robotic Systems*. Springer, 2019, pp. 99–110.
- [8] M. Park, Y. Ohm, D. Kim, and Y.-L. Park, "Multi-material soft strain sensors with high gauge factors for proprioceptive sensing of soft bending actuators," in *2019 2nd IEEE International Conference on Soft Robotics (RoboSoft)*. IEEE, 2019, pp. 384–390.
- [9] L. Wang and Z. Wang, "Mechanoreception for soft robots via intuitive body cues," *Soft robotics*, vol. 7, no. 2, pp. 198–217, 2020.
- [10] H. Wang, M. Totaro, and L. Beccai, "Toward perceptive soft robots: Progress and challenges," *Advanced Science*, vol. 5, no. 9, p. 1800541, 2018.
- [11] S. E. Navarro, S. Nagels, H. Alagi, L.-M. Faller, O. Goury, T. Morales-Bieze, H. Zangl, B. Hein, R. Ramakers, W. Deferme, et al., "A model-based sensor fusion approach for force and shape estimation in soft robotics," *IEEE Robotics and Automation Letters*, vol. 5, no. 4, pp. 5621–5628, 2020.
- [12] M. Hofer, C. Sferrazza, and R. D'Andrea, "A vision-based sensing approach for a spherical soft robotic arm," *Frontiers in Robotics and AI*, vol. 8, p. 630935, 2021.
- [13] J. M. Bern, Y. Schneider, P. Banzet, N. Kumar, and S. Coros, "Soft robot control with a learned differentiable model," in *2020 3rd IEEE International Conference on Soft Robotics (RoboSoft)*. IEEE, 2020, pp. 417–423.
- [14] A. AlBeladi, G. Krishnan, M.-A. Belabbas, and S. Hutchinson, "Vision-based shape reconstruction of soft continuum arms using a geometric strain parametrization," in *2021 IEEE International Conference on Robotics and Automation (ICRA)*. IEEE, 2021, pp. 11 753–11 759.
- [15] F. Xu, H. Wang, W. Chen, and Y. Miao, "Visual servoing of a cable-driven soft robot manipulator with shape feature," *IEEE Robotics and Automation Letters*, vol. 6, no. 3, pp. 4281–4288, 2021.
- [16] C. Duriez, "Control of elastic soft robots based on real-time finite element method," in *2013 IEEE international conference on robotics and automation*. IEEE, 2013, pp. 3982–3987.
- [17] A. D. Marchese, K. Komorowski, C. D. Onal, and D. Rus, "Design and control of a soft and continuously deformable 2d robotic manipulation system," in *2014 IEEE international conference on robotics and automation (ICRA)*. Ieee, 2014, pp. 2189–2196.
- [18] R. K. Katzschmann, C. Della Santina, Y. Toshimitsu, A. Bicchì, and D. Rus, "Dynamic motion control of multi-segment soft robots using piecewise constant curvature matched with an augmented rigid body model," in *2019 2nd IEEE International Conference on Soft Robotics (RoboSoft)*. IEEE, 2019, pp. 454–461.
- [19] A. Patrizi, E. Pennestri, and P. P. Valentini, "Comparison between low-cost marker-less and high-end marker-based motion capture systems for the computer-aided assessment of working ergonomics," *Ergonomics*, vol. 59, no. 1, pp. 155–162, 2016.
- [20] M. W. Hannan and I. D. Walker, "Real-time shape estimation for continuum robots using vision," *Robotica*, vol. 23, no. 5, pp. 645–651, 2005.
- [21] D. B. Camarillo, K. E. Loewke, C. R. Carlson, and J. K. Salisbury, "Vision based 3-d shape sensing of flexible manipulators," in *2008 IEEE International Conference on Robotics and Automation*. IEEE, 2008, pp. 2940–2947.
- [22] J. M. Croom, D. C. Rucker, J. M. Romano, and R. J. Webster, "Visual sensing of continuum robot shape using self-organizing maps," in *2010 IEEE International Conference on Robotics and Automation*. IEEE, 2010, pp. 4591–4596.
- [23] E. Ceseracciu, Z. Sawacha, and C. Cobelli, "Comparison of markerless and marker-based motion capture technologies through simultaneous data collection during gait: proof of concept," *PloS one*, vol. 9, no. 3, p. e87640, 2014.
- [24] A. Vandini, C. Bergeles, B. Glocker, P. Giataganas, and G.-Z. Yang, "Unified tracking and shape estimation for concentric tube robots," *IEEE Transactions on Robotics*, vol. 33, no. 4, pp. 901–915, 2017.
- [25] A. Vandini, B. Glocker, M. Hamady, and G.-Z. Yang, "Robust guidewire tracking under large deformations combining segment-like features (seglets)," *Medical image analysis*, vol. 38, pp. 150–164, 2017.
- [26] A. Reiter, A. Bajo, K. Iliopoulos, N. Simaan, and P. K. Allen, "Learning-based configuration estimation of a multi-segment continuum robot," in *2012 4th IEEE RAS & EMBS International Conference on Biomedical Robotics and Biomechanics (BioRob)*. IEEE, 2012, pp. 829–834.
- [27] A. Mathis, P. Mamidanna, K. M. Cury, T. Abe, V. N. Murthy, M. W. Mathis, and M. Bethge, "DeepLabcut: markerless pose estimation of user-defined body parts with deep learning," *Nature neuroscience*, vol. 21, no. 9, pp. 1281–1289, 2018.
- [28] P. Werner, M. Hofer, C. Sferrazza, and R. D'Andrea, "Vision-based proprioceptive sensing for soft inflatable actuators," *arXiv preprint arXiv:1909.09096*, 2019.
- [29] R. Wang, S. Wang, S. Du, E. Xiao, W. Yuan, and C. Feng, "Real-time soft body 3d proprioception via deep vision-based sensing," *IEEE Robotics and Automation Letters*, vol. 5, no. 2, pp. 3382–3389, 2020.
- [30] Y. She, S. Q. Liu, P. Yu, and E. Adelson, "Exoskeleton-covered soft finger with vision-based proprioception and tactile sensing," in *2020 IEEE International Conference on Robotics and Automation (ICRA)*. IEEE, 2020, pp. 10 075–10 081.
- [31] N. Otsu, "A threshold selection method from gray-level histograms," *IEEE transactions on systems, man, and cybernetics*, vol. 9, no. 1, pp. 62–66, 1979.
- [32] K. Simonyan and A. Zisserman, "Very deep convolutional networks for large-scale image recognition," *arXiv preprint arXiv:1409.1556*, 2014.
- [33] R. J. Webster III and B. A. Jones, "Design and kinematic modeling of constant curvature continuum robots: A review," *The International Journal of Robotics Research*, vol. 29, no. 13, pp. 1661–1683, 2010.
- [34] C. Della Santina, A. Bicchì, and D. Rus, "On an improved state parametrization for soft robots with piecewise constant curvature and its use in model based control," *IEEE Robotics and Automation Letters*, vol. 5, no. 2, pp. 1001–1008, 2020.
- [35] E. Olson, "Apriltag: A robust and flexible visual fiducial system," in *2011 IEEE international conference on robotics and automation*. IEEE, 2011, pp. 3400–3407.
- [36] Y. Toshimitsu, K. W. Wong, T. Buchner, and R. Katzschmann, "Sopra: Fabrication & dynamical modeling of a scalable soft continuum robotic arm with integrated proprioceptive sensing," in *2021 IEEE/RSJ International Conference on Intelligent Robots and Systems (IROS)*. IEEE, 2021, pp. 653–660.
- [37] Y. Zhang and R. K. Katzschmann, "Creation of a modular soft robotic fish testing platform," *arXiv preprint arXiv:2201.04098*, 2022.
- [38] O. Fischer, Y. Toshimitsu, A. Kazempour, and R. K. Katzschmann, "Dynamic task space control enables soft manipulators to perform real-world tasks," *Advanced Intelligent Systems*, p. 2200024.
- [39] J. Z. Zhang, Y. Zhang, P. Ma, E. Nava, T. Du, P. Arm, W. Matusik, and R. K. Katzschmann, "Learning material parameters and hydrodynamics of soft robotic fish via differentiable simulation," *arXiv preprint arXiv:2109.14855*, 2021.
- [40] L. Keselman, J. Iselin Woodfill, A. Grunnet-Jepsen, and A. Bhowmik, "Intel realsense stereoscopic depth cameras," in *Proceedings of the IEEE conference on computer vision and pattern recognition workshops*, 2017, pp. 1–10.
- [41] Y. Pedari, A. Parvaresh, and S. A. A. Moosavian, "Spatial shape estimation of a tendon-driven continuum robotic arm using a vision-based algorithm," in *2019 7th International Conference on Robotics and Mechatronics (ICRoM)*. IEEE, 2019, pp. 625–630.
- [42] K. Amano, N. Goda, S. Nishida, Y. Ejima, T. Takeda, and Y. Ohtani, "Estimation of the timing of human visual perception from magnetoencephalography," *Journal of Neuroscience*, vol. 26, no. 15, pp. 3981–3991, 2006.